

Dalton Transactions

Accepted Manuscript



This is an *Accepted Manuscript*, which has been through the Royal Society of Chemistry peer review process and has been accepted for publication.

Accepted Manuscripts are published online shortly after acceptance, before technical editing, formatting and proof reading. Using this free service, authors can make their results available to the community, in citable form, before we publish the edited article. We will replace this *Accepted Manuscript* with the edited and formatted *Advance Article* as soon as it is available.

You can find more information about *Accepted Manuscripts* in the [Information for Authors](#).

Please note that technical editing may introduce minor changes to the text and/or graphics, which may alter content. The journal's standard [Terms & Conditions](#) and the [Ethical guidelines](#) still apply. In no event shall the Royal Society of Chemistry be held responsible for any errors or omissions in this *Accepted Manuscript* or any consequences arising from the use of any information it contains.

Seven phenoxido-bridged complexes encapsulated by 8-hydroxyquinoline Schiff base derivatives and β -diketone ligands: single-molecule magnet, magnetic refrigeration and luminescence properties

Shi-Yu Wang, Wen-Min Wang, Hong-Xia Zhang, Hai-Yun Shen, Li Jiang, Jian-Zhong Cui* and Hong-Ling Gao*

Abstract

Seven dinuclear complexes based on 8-hydroxyquinoline Schiff base derivatives and β -diketone ligands, $[\text{RE}_2(\text{hfac})_4\text{L}_2]$ (RE = Y (**1**), Gd (**2**), Tb (**3**), Dy (**4**), Ho (**5**), Er (**6**) and Lu (**7**); hfac^- = hexafluoroacetylacetonate; HL = 2-[(4-chloro-phenylimino)-methyl]-8-hydroxyquinoline), have been synthesized, structurally and magnetically characterized. Complexes **1–7** have similar dinuclear structures, in which each RE^{III} ion is eight coordinated by two L^- and two hfac^- ligands in a distorted dodecahedron geometry. The luminescence spectra indicate that complex **3** exhibits characteristic Tb^{III} ion luminescence, while **1** and **7** show HL ligand luminescence. The magnetic studies reveal that **2** features magnetocaloric effect with the magnetic entropy change of $-\Delta S_m = 16.83 \text{ J kg}^{-1} \text{ K}^{-1}$ at 2 K for $\Delta H = 8 \text{ T}$, and **4** displays slow magnetic relaxation behavior with the anisotropic barrier of 6.7 K and pre-exponential factor $\tau_0 = 5.3 \times 10^{-6} \text{ s}$.

Introduction

In recent years, the great interest has been shown in the studies of cluster-based magnetic materials due to their fascinating applications in fields such as single-molecule magnets (SMMs) and molecular coolers with the magnetocaloric effect (MCE).^{1,2} The origin of the

* Department of Chemistry, Tianjin University, Tianjin 300072, P. R. China. E-mail: cuijianzhong@tju.edu.cn

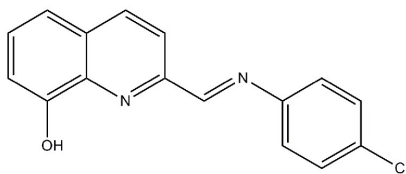
* Department of Chemistry, Tianjin University, Tianjin 300072, P. R. China. E-mail: ghl@tju.edu.cn

SMM behavior is the easy axis magnetic anisotropy ($D < 0$), which causes the formation of an energy barrier that prevents the reversal of the molecular magnetization and causes a slow relaxation of the magnetization at low temperature.³ Since the discovery in the early 1990s of the first single molecule magnet (SMM), $[\text{Mn}_{12}]$ acetate,³ a large number of complexes displaying this property have been reported. Most of them, especially in the early years, contain only 3d ions.⁴ Following the increased knowledge of the magnetochemical properties of SMMs, lanthanide (Ln) ions have become good candidates for the preparation of such materials because most of them have a large unquenched orbital angular momentum,⁵ which may bring significant anisotropy to the system. Many polymetallic Ln-SMMs, the majority based on Dy^{III} , have also been reported, some of which show impressive SMM properties, such as high values of anisotropic barrier and/or blocking temperatures.⁶ The dilanthanide SMMs $[\text{Ln}_2\{\text{N}(\text{SiMe}_3)_2\}_4(\text{thf})_2(\mu\text{:}\eta^2\text{:}\eta^2\text{-N}_2)]^-$ with Ln = Dy or Tb, reported by Evans, Long et al., attracted a great deal of attention because the Ln^{III} ions are strongly exchange-coupled by the radical $[\text{N}_2]^{3-}$ ligand.⁷ In 2012, Tune et al. reported the first sulfur-bridged $\{\text{Dy}_2\}$ SMM $[\{\text{Cp}'_2\text{Dy}(\mu\text{-SSiPh}_3)\}_2]$ with a high magnetization reversal barrier of 192 K.⁸

Magnetic refrigeration, based on the magnetocaloric effect (MCE), has received much interest recently due to the possibility of replacing the expensive and increasingly rare He-3 in ultralow-temperature refrigeration.⁹ In this regard, Gd^{III} cluster complexes are promising candidates.¹⁰ On the one hand, the magnetic interaction between Gd^{III} ions is expected to be very weak because of the shielding of the f orbitals and the consequent poor overlap with bridging ligand orbitals.¹¹ On the other hand, a large S of an isotropic Gd^{III} ion provides the largest entropy per single ion.¹² Additionally, various structures of discrete Gd-clusters have

been observed, such as Gd₂,^{13(a)} Gd₂₄,^{13(b)} Gd₄₈,^{13(c)} Gd₁₀₄.^{13(d)}

A well-selected ligand is one of the key factors in building lanthanide-based magnetic materials. 8-hydroxyquinoline derivatives attracted great interest in constructing 4f SMMs in recent years.¹⁴ Accordingly, we selected the 2-[(4-chloro-phenylimino)-methyl]-8-hydroxyquinoline (HL, Scheme 1) as the ligand, the phenoxide oxygen atom can be deprotonated to act as a bridge between metal centers, which may propagate magnetic coupling between paramagnetic ions efficiently. In addition, to promote the encapsulation of metal ions, RE(hfac)₃·2H₂O (hfac⁻ = hexafluoroacetylacetonate) was used as the metal precursor in our reaction mixtures. Especially, 8-hydroxyquinoline and its derivatives and β-diketone have been successfully used in the construction of fluorescent materials,¹⁵ so it is promising to obtain multifunctional materials correlating the magnetic and luminescence properties. Here we report the assembly of seven phenoxido-bridged dinuclear complexes [RE₂(hfac)₄L₂] (RE = Y (**1**), Gd (**2**), Tb (**3**), Dy (**4**), Ho (**5**), Er (**6**) and Lu (**7**)). Magnetic measurements on complexes **2–6** were carried out. Magnetic studies reveal single-molecule magnet (SMM) behavior for **4**; meanwhile, complex **2** displays a magnetocaloric effect. The luminescence properties of **1**, **3**, **4** and **7** were also investigated.



Scheme 1. Structure of ligand HL

Experimental section

General Methods and Materials. RE(hfac)₃·2H₂O (RE = Y, Gd, Tb, Dy, Ho, Er and Lu)

were synthesized according to methods in the literature.¹⁶ 2-[(4-chloro-phenylimino)-methyl]-8-hydroxyquinoline (HL) was prepared by the reported methods.¹⁷ Other chemical reagents and solvents were of analytical-grade quality, obtained from commercial sources, and used without further purification. Elemental analyses for C, H and N were carried out on a Perkin-Elmer 240 CHN elemental analyzer. Infrared spectra (IR) of the complexes in KBr pellets were obtained on a Bruker Tensor 27 IR spectrometer in the range of 4000–400 cm^{-1} region. UV-vis spectra were performed on a TU-1901 spectrophotometer at room temperature. Fluorescence spectra were taken on a Cary Eclipse fluorescence spectrophotometer supplied by Varian (USA) at room temperature. Powder X-ray diffraction (PXRD) data were performed on a Rigaku D/max 2500v/pc X-ray powder diffractometer with Cu-K α radiation ($\lambda = 1.540598 \text{ \AA}$), with a scan speed of 5° min^{-1} in the range $2\theta = 5\text{--}50^\circ$. Thermal gravimetric analyses (TGA) were carried out on a NETZSCH TG 209 instrument under air atmosphere from 30 to 800 $^\circ\text{C}$ with a heating rate of $10^\circ\text{C}\cdot\text{min}^{-1}$. The magnetic measurements were carried out with a Quantum Design MPMS-XL7 and a PPMS-9 ACMS magnetometer. The diamagnetic corrections for the complexes were estimated using Pascal's constants and magnetic data were corrected for diamagnetic contributions of the sample holder.

Synthesis of $[\text{RE}_2(\text{hfac})_4\text{L}_2]$ (RE = Y (1), Gd (2), Tb (3), Dy (4), Ho (5), Er (6) and Lu (7)). Complexes 1–7 were prepared by using similar procedures. A solution of $\text{RE}(\text{hfac})_3\cdot 2\text{H}_2\text{O}$ (0.025 mmol) in 20 mL boiling heptane was heated to reflux for 2 h. Then the solution was cooled to 70 $^\circ\text{C}$, and a CH_2Cl_2 (5 mL) solution of HL (0.025 mmol) was added. The resulting mixture was stirred for 30 min at this temperature, and then cooled it to room temperature. The mixture was filtrated and the filtrate was kept in the dark and

concentrated slowly by evaporation at 4 °C. After three days, red crystals were collected, washed with heptane and dried in air.

[Y₂(hfac)₄L₂] (1). Yield: ca. 62% (based on Y³⁺). Elemental analysis (%) Calcd for C₅₂H₂₄Cl₂F₂₄N₄O₁₀Y₂ (*Mr*, 1569.47): C 39.75, H 1.54, N 3.57. Found: C 39.88, H 1.58, N 3.62. IR (cm⁻¹): 1656 (s), 1594 (w), 1552 (w), 1483 (m), 1463 (m), 1255 (s), 1200 (s), 1137 (s), 1096 (m).

[Gd₂(hfac)₄L₂] (2). Yield: ca. 58% (based on Gd³⁺). Elemental analysis (%) Calcd for C₅₂H₂₄Cl₂F₂₄N₄O₁₀Gd₂ (*Mr*, 1706.16): C 36.61, H 1.42, N 3.28. Found: C 36.78, H 1.53, N 3.31. IR (cm⁻¹): 1650 (s), 1597 (w), 1547 (w), 1476 (m), 1460 (m), 1251 (s), 1200 (s), 1147 (s), 1096 (m).

[Tb₂(hfac)₄L₂] (3). Yield: ca. 54% (based on Tb³⁺). Elemental analysis (%) Calcd for C₅₂H₂₄Cl₂F₂₄N₄O₁₀Tb₂ (*Mr*, 1709.5): C 36.54, H 1.42, N 3.28. Found: C 36.43, H 1.47, N 3.38. IR (cm⁻¹): 1653 (s), 1600 (w), 1551 (w), 1482 (m), 1459 (m), 1251 (s), 1198 (s), 1141 (s), 1098 (m).

[Dy₂(hfac)₄L₂] (4). Yield: ca. 60% (based on Dy³⁺). Elemental analysis (%) Calcd for C₅₂H₂₄Cl₂F₂₄N₄O₁₀Dy₂ (*Mr*, 1716.66): C 36.38, H 1.41, N 3.26. Found: C 36.21, H 1.49, N 3.39. IR (cm⁻¹): 1650 (s), 1601 (w), 1552 (w), 1483 (m), 1463 (m), 1255 (s), 1200 (s), 1144 (s), 1096 (m).

[Ho₂(hfac)₄L₂] (5). Yield: ca. 65% (based on Ho³⁺). Elemental analysis (%) Calcd for C₅₂H₂₄Cl₂F₂₄N₄O₁₀Ho₂ (*Mr*, 1721.52): C 36.28, H 1.41, N 3.26. Found: C 36.41, H 1.38, N 3.32. IR (cm⁻¹): 1656 (s), 1594 (w), 1560 (w), 1483 (m), 1463 (m), 1255 (s), 1200 (s), 1137

(s), 1096 (m).

[Er₂(hfac)₄L₂] (6). Yield: ca. 55% (based on Er³⁺). Elemental analysis (%) Calcd for C₅₂H₂₄Cl₂F₂₄N₄O₁₀Er₂ (*Mr*, 1726.18): C 36.18, H 1.40, N 3.25. Found: C 36.27, H 1.32, N 3.19. IR (cm⁻¹): 1655 (s), 1603 (w), 1552 (w), 1483 (m), 1460 (m), 1249 (s), 1200 (s), 1143 (s), 1097 (m).

[Lu₂(hfac)₄L₂] (7). Yield: ca. 65% (based on Lu³⁺). Elemental analysis (%) Calcd for C₅₂H₂₄Cl₂F₂₄N₄O₁₀Lu₂ (*Mr*, 1741.6): C 35.86, H 1.39, N 3.22. Found: C 35.68, H 1.44, N 3.16. IR (cm⁻¹): 1656 (s), 1601 (w), 1550 (w), 1483 (m), 1463 (m), 1255 (s), 1200 (s), 1147 (s), 1096 (m).

X-ray crystallography

Single crystal X-ray diffraction data of **1–7** were collected on a computer-controlled Rigaku Saturn CCD area detector diffractometer, equipped with confocal monochromatized Mo-K α radiation with a radiation wavelength of 0.71073 Å using the ω - ϕ scan technique. CrystalClear software was used for the collection, processing, and correction for Lorentzian and polarization effects.¹⁸ An absorption correction was applied based on comparison of multiple symmetry equivalent measurements. The structures were solved using a direct method and refined anisotropically using a full-matrix least-squares method based on F^2 with the SHELXL program package for all of the non-hydrogen atoms.¹⁹ Hydrogen atoms were located and included at their calculated positions. In both **2** and **3** there exist some higher residue peaks (the largest: 3.66×10^3 , 2.06×10^3 e \cdot nm⁻³) which appear near the O3 atoms in **2** and **3**, show no obvious chemical significance. The details of the crystal parameters, data

collection and refinements for the complexes are summarized in Table 1. Selected bond distances [\AA] and angles [deg] are given in Table 2. CCDC 1427272 (**1**), 1427268 (**2**), 1427271 (**3**), 1427266 (**4**), 1427269 (**5**), 1427267 (**6**), and 1427270 (**7**) include all supplementary crystallographic data of seven complexes. These data can be obtained free of charge from the Cambridge Crystallographic Data Center via www.ccdc.cam.ac.uk/data_request/cif.

Results and discussion

Crystal Structures of $[\text{RE}_2(\text{hfac})_4\text{L}_2]$ X-ray diffraction analysis reveals that **1–7** are isomorphic dinuclear complexes and crystallize in the monoclinic $P2(1)/n$ space group, so as a representative, the structure of **4** will be described in detail. Complex **4** is composed of two 8-coordinated Dy^{III} ions bridged by two $\mu_2\text{-O}$ of the L^- ligands, as displayed in Figure 1a. Each Dy^{III} ion is bound by two L^- ligands (O1, O1a, N1 and N2) and two hfac^- ligands (O2, O3, O4 and O5). The Dy^{III} centers adopt a distorted dodecahedron geometry (Figure 1b). The pentagonal plane is composed of the ligand atoms O1, O1a, O3, N1 and N2, while the interpenetrating triangle is composed of O2, O4 and O5. The r.m.s. deviation of the atoms that form the pentagonal plane (O1, O1a, O3, N1 and N2) is 0.1653 and the deviation of the Dy^{III} atom from that plane is 0.6180 \AA . Phenoxide oxygen atoms (O1 and O1a) of the L^- ligands bridge the two Dy^{III} centers, giving rise to a four-membered Dy_2O_2 rhomboid (Figure 1c), which exhibits a center of symmetry with Dy–O bond lengths of 2.290(2), 2.364(2) \AA , Dy \cdots Dy distance of 3.7581(7) \AA and two Dy–O–Dy angles of 107.71(6) $^\circ$.

The packing arrangement along the *b* axis of **4** is shown in Figure 1(d). Along the *b* axis, it can be seen that the dinuclear complex is well-isolated, with the smallest intermolecular

Dy \cdots Dy distance being 10.8482(2) Å and the smallest intramolecular Dy1 \cdots Dy1a distance being 3.7581(7) Å. The packing along the *a* and *c* axes can be found in Figure S1 (ESI). The well-isolated molecules are aligned in a parallel fashion along all crystallographic axes.

As displayed in Table 2, for complexes 2–7, the Ln–O_{average} bond lengths, Ln–N_{average} bond lengths, and the distances of Ln \cdots Ln decrease as the ionic radius of the Ln^{III} cations decrease, which originates from the effect of the lanthanide contraction.²⁰ Moreover, these Ln–O, Ln–N bond distances are comparable to those of the reported in other phenoxido-bridged lanthanide complexes.²¹

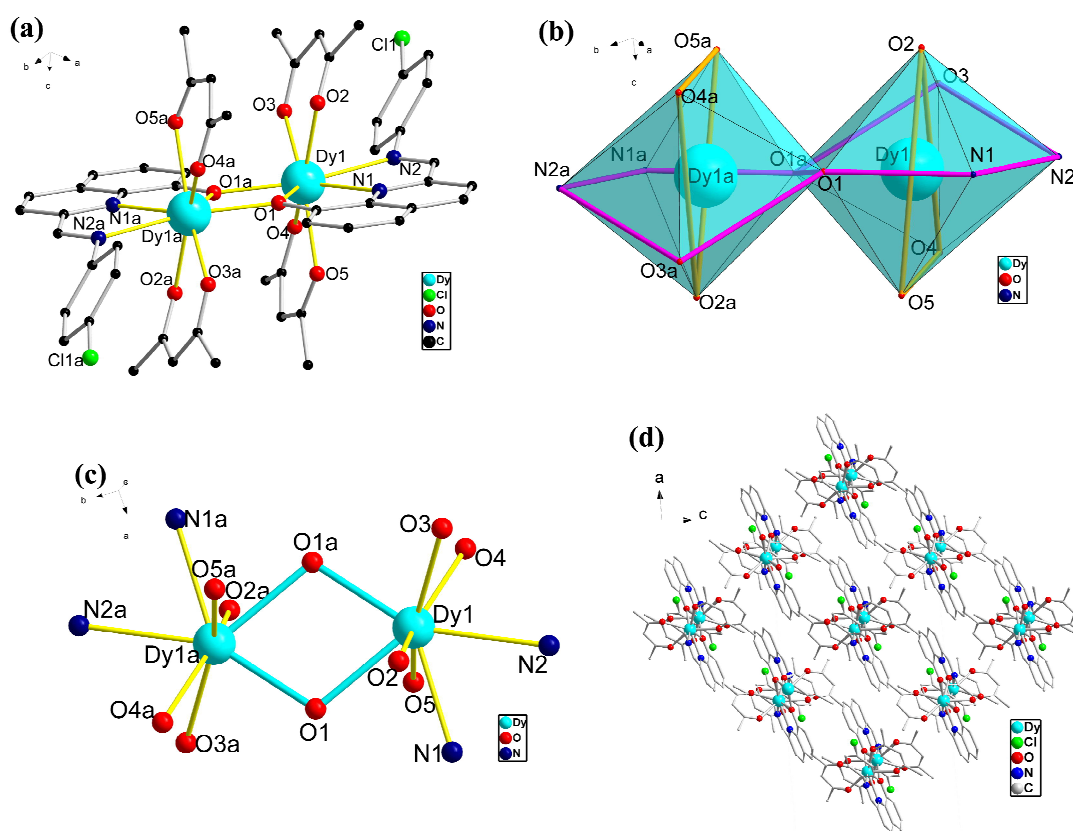


Figure 1. (a) Molecular structure of $[\text{Dy}_2(\text{hfac})_4\text{L}_2]$ (Hydrogen and fluorine atoms are omitted for clarity); (b) coordination polyhedra of the Dy^{III} ions in complex 4; (c) dinuclear core structure of complex 4; (d) packing arrangement of complex 4 viewed along the crystallographic *b* axis.

Table 1. Crystallographic data and processing parameters for complexes 1–7

Complex	1	2	3	4	5	6	7
Formula	C ₅₂ H ₂₄ Cl ₂ F ₂₄ N ₄ O ₁₀ Y ₂	C ₅₂ H ₂₄ Cl ₂ F ₂₄ N ₄ O ₁₀ Gd ₂	C ₅₂ H ₂₄ Cl ₂ F ₂₄ N ₄ O ₁₀ Tb ₂	C ₅₂ H ₂₄ Cl ₂ F ₂₄ N ₄ O ₁₀ Dy ₂	C ₅₂ H ₂₄ Cl ₂ F ₂₄ N ₄ O ₁₀ Ho ₂	C ₅₂ H ₂₄ Cl ₂ F ₂₄ N ₄ O ₁₀ Er ₂	C ₅₂ H ₂₄ Cl ₂ F ₂₄ N ₄ O ₁₀ Lu ₂
Formula weight	1569.47	1706.15	1709.49	1716.65	1721.51	1726.17	1741.59
Temperature (K)	113(2)	113(2)	113(2)	113(2)	113(2)	113(2)	113(2)
Wavelength (Å)	0.71073	0.71073	0.71073	0.71073	0.71073	0.71073	0.71073
Crystal system	Monoclinic	Monoclinic	Monoclinic	Monoclinic	Monoclinic	Monoclinic	Monoclinic
Space group	P2(1)/n	P2(1)/n	P2(1)/n	P2(1)/n	P2(1)/n	P2(1)/n	P2(1)/n
<i>a</i> (Å)	11.380(2)	11.348(2)	11.345(2)	11.347(2)	11.361(2)	11.393(2)	11.416(2)
<i>b</i> (Å)	19.207(4)	19.320(4)	19.264(4)	19.187(4)	19.160(4)	19.181(4)	19.038(4)
<i>c</i> (Å)	13.089(3)	13.115(3)	13.074(3)	13.041(3)	13.035(3)	13.054(3)	12.998(3)
α (deg)	90	90	90	90	90	90	90
β (deg)	95.04(3)	95.21(3)	95.17(3)	95.15(3)	95.15(3)	95.10(3)	94.99(3)
γ (deg)	90	90	90	90	90	90	90
Volume (Å ³)	2849.9(10)	2863.6(10)	2845.7(10)	2827.7(10)	2825.9(10)	2841.6(10)	2814.1(10)
<i>Z</i>	2	2	2	2	2	2	2
Calculated density (Mg m ⁻³)	1.829	1.979	1.995	2.016	2.023	2.017	2.055
Absorption coefficient (mm ⁻¹)	2.260	2.529	2.699	2.858	3.016	3.168	3.725
<i>F</i> (000)	1544	1644	1648	1652	1656	1660	1672
θ range for data collection (deg)	1.89 to 25.02	1.88 to 27.93	1.89 to 28.01	2.12 to 27.94	1.89 to 27.94	1.89 to 27.89	1.90 to 25.02
Reflections collected	26187	25700	29090	27956	28448	32905	23448
Independent reflection	5026 [<i>R</i> (int) = 0.0456]	6827 [<i>R</i> (int) = 0.0627]	6792 [<i>R</i> (int) = 0.0566]	6750 [<i>R</i> (int) = 0.0307]	6763 [<i>R</i> (int) = 0.0421]	6769 [<i>R</i> (int) = 0.0428]	4979 [<i>R</i> (int) = 0.0491]
Data / restraints / parameters	5026 / 91 / 445	6827 / 223 / 481	6792 / 66 / 452	6750 / 223 / 481	6763 / 127 / 481	6769 / 217 / 481	4979 / 6 / 424
Goodness-of-fit on <i>F</i> ²	1.064	1.087	1.105	1.097	1.056	1.117	1.061
Final <i>R</i> indices [<i>I</i> > 2 σ (<i>I</i>)]	<i>R</i> ₁ = 0.0373, <i>wR</i> ₂ = 0.0837	<i>R</i> ₁ = 0.0468, <i>wR</i> ₂ = 0.1100	<i>R</i> ₁ = 0.0440, <i>wR</i> ₂ = 0.0831	<i>R</i> ₁ = 0.0248, <i>wR</i> ₂ = 0.0590	<i>R</i> ₁ = 0.0315, <i>wR</i> ₂ = 0.0631	<i>R</i> ₁ = 0.0289, <i>wR</i> ₂ = 0.0613	<i>R</i> ₁ = 0.0322, <i>wR</i> ₂ = 0.0654
<i>R</i> indices (all data)	<i>R</i> ₁ = 0.0437, <i>wR</i> ₂ = 0.0873	<i>R</i> ₁ = 0.0565, <i>wR</i> ₂ = 0.1176	<i>R</i> ₁ = 0.0566, <i>wR</i> ₂ = 0.0883	<i>R</i> ₁ = 0.0293, <i>wR</i> ₂ = 0.0611	<i>R</i> ₁ = 0.0414, <i>wR</i> ₂ = 0.0670	<i>R</i> ₁ = 0.0344, <i>wR</i> ₂ = 0.0639	<i>R</i> ₁ = 0.0410, <i>wR</i> ₂ = 0.0694

Table 2. Selected bond lengths (Å) and angles (°) for complexes **1–7**

	1	2	3	4	5	6	7
RE1–O1	2.281(2)	2.323(3)	2.301(3)	2.290(2)	2.279(2)	2.274(2)	2.241(3)
RE1–O1a	2.356(2)	2.386(3)	2.375(3)	2.364(2)	2.349(2)	2.346(2)	2.326(3)
RE1–O2	2.344(2)	2.383(3)	2.361(3)	2.345(2)	2.338(2)	2.335(2)	2.296(3)
RE1–O3	2.356(2)	2.396(3)	2.378(3)	2.367(2)	2.352(2)	2.346(2)	2.315(3)
RE1–O4	2.334(2)	2.378(3)	2.354(3)	2.344(2)	2.331(2)	2.325(2)	2.294(3)
RE1–O5	2.370(2)	2.404(3)	2.391(3)	2.373(2)	2.362(2)	2.359(2)	2.325(3)
RE–O _{average}	2.340(2)	2.378(3)	2.360(3)	2.347(2)	2.335(2)	2.331(2)	2.300(3)
RE1–N1	2.434(3)	2.471(4)	2.450(3)	2.435(2)	2.422(3)	2.419(2)	2.384(4)
RE1–N2	2.610(3)	2.636(3)	2.626(3)	2.607(2)	2.599(3)	2.597(2)	2.577(4)
RE–N _{average}	2.522(3)	2.554(4)	2.538(4)	2.521(2)	2.511(3)	2.508(2)	2.481(4)
RE···RE	3.7502(9)	3.8040(8)	3.7731(8)	3.7582(7)	3.7451(7)	3.7413(7)	3.6958(8)
RE–O–RE	107.93(7)	107.75(10)	107.59(10)	107.71(6)	108.05(8)	108.13(7)	108.01(11)

Powder X-ray Diffraction (PXRD) and Thermal gravimetric Analysis (TGA).

In order to prove that the crystal structures of complexes **1–7** are truly representative of their bulk materials, PXRD experiments were carried out on the as-synthesized samples. As shown in Figure S2–S8 (ESI), the experimental PXRD patterns for **1–7** are in good accordance with the simulated PXRD patterns from the data of single-crystal X-ray diffraction, suggesting high phase purity of the bulk materials for **1–7**. The different intensities between the simulated and experimental PXRD patterns may be ascribed to the variation in preferred orientation of the powder.

The thermal stabilities were studied on the crystalline samples for **1–7** (Figure S9, ESI). All the TG curves have the similar profiles, exhibiting two main weight loss steps. Herein, **4** is used as representative illustrated in Figure 2. The TG curve of **4** indicates the thermal stability up to 286 °C, and then the first weight loss of 32.95% from 286 to 335 °C may be attributed to the loss of two 8-hydroxyquinoline Schiff base ligands (L⁻) (calcd 32.82%). The second weight loss of 44%, occurring at the temperature range of 335 to 583 °C, corresponds

to the loss of hfac^- ligands (calcd 45.45%). Finally, the residue of 23.05% shows Dy_2O_3 component (calcd 21.73%).

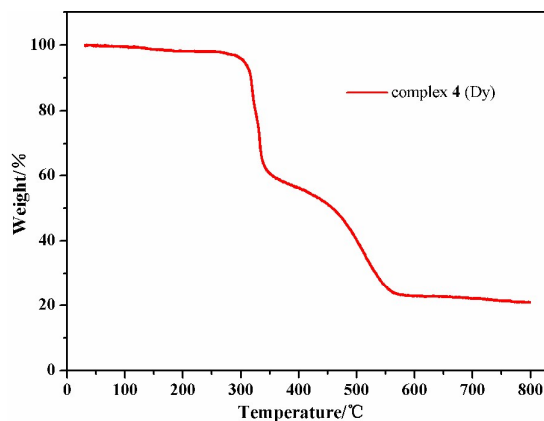


Figure 2. TG curve of complex 4.

UV-Vis Spectra and Photoluminescent Properties.

The UV-vis spectra of free ligand HL, $\text{Dy}(\text{hfac})_3 \cdot 2\text{H}_2\text{O}$ and complexes **1–7** were performed in methanol solutions of 10^{-5} mol/L in the wavelength range of 200–600 nm at room temperature. As shown in Figure S10 (ESI), the ligand HL displays three absorption peaks at 210, 247 and 342 nm in the UV region, attributed to singlet-singlet $n \rightarrow \pi^*$ and $\pi \rightarrow \pi^*$ transitions of the aromatic rings. $\text{Dy}(\text{hfac})_3 \cdot 2\text{H}_2\text{O}$ behaves a strong characteristic absorption at 300 nm. For **1–7**, the absorption peak at 216 nm and the broad low-energy absorption at 365 nm are due to the L^- ligand, note that the two absorption bands in **1–7** have a slight red shift relative to that of the free ligand and the absorption peak at 247 nm of HL ligand has disappeared when coordinated with RE^{III} cations, which can be ascribed to the coordination effect between the ligand L^- and RE^{III} cations. The observed intense absorption at 300 nm in **1–7** should be ascribed to hfac^- .

The luminescent properties of HL ligand and complexes **1**, **3**, **4** and **7** in methanol solutions of 10^{-5} mol/L were investigated at room temperature. Under excitation at 250 nm for HL, the pure ligand presents three emissions with the peaks at 319, 350 and 623 nm (Figure 3a). It is obviously that three emission bands centered at 321, 350 and 623 nm were observed for complexes **1** and **7** on excitation at 250 nm, which are assigned to the ligand luminescence. It is well-known that among the rare earth elements, Y^{3+} has an empty 4f shell and Lu^{3+} ion has a filled 4f shell, thus no f-f transitions occur and consequently, no typical emission in the visible range of the spectra can be observed.

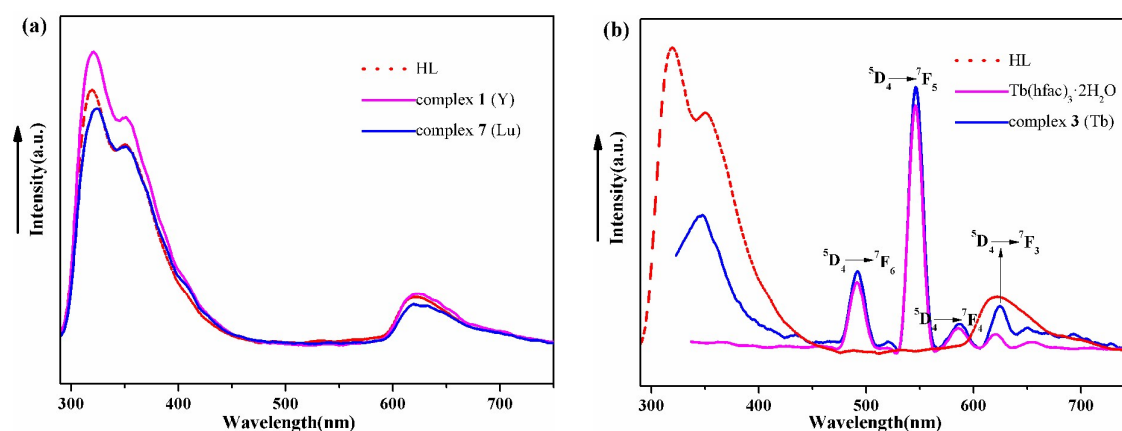


Figure 3. (a) The emission spectra of HL, complexes **1** and **7** in methanol solutions; (b) the emission spectra of HL, $Tb(hfac)_3 \cdot 2H_2O$ and complex **3** in methanol solutions.

As shown in Figure 3(b), the emission spectrum of complex **3** exhibits the typical emission bands of Tb^{3+} ion, upon excitation at 313 nm, centered at 492, 546, 587 and 621 nm, which are assigned to the $^5D_4 \rightarrow ^7F_6$, $^5D_4 \rightarrow ^7F_5$, $^5D_4 \rightarrow ^7F_4$ and $^5D_4 \rightarrow ^7F_3$ transitions, respectively. Moreover, a broad band centered at 348 nm is also detected. The photosensitized emission is initiated by the excitation of the ground state of the ligand containing a photosensitizer to its excited singlet state, followed by intersystem crossing to the excited

triplet state. Then, the excitation energy of the excited triplet state is transferred to the lanthanide ions, resulting in the emission.²² To make energy transfer effective, the triplet states of the ligand and the accepting lanthanide energy level should be matched. According to Latva's empirical rule,²³ an optimal ligand-to-metal energy transfer process for Ln^{III} needs an energy gap ΔE and the ΔE value that gives the maximum emission quantum yield is not zero but has a certain value. The lowest excited energy level of the Tb^{III} ion is located at 20500 cm⁻¹ (⁵D₄). However, 8-hydroxyquinoline and its derivatives have low energy triplet states at approximately 17100 cm⁻¹ which cannot transfer energy to Tb^{III} effectively.²⁴ However, the triplet energy level of the hexafluoroacetylacetonate ligand (22200 cm⁻¹) lies above the resonant level of Tb^{III} with the ΔE of 1700 cm⁻¹, allowing an efficient ligand-to-metal energy transfer. Thus, the emission spectrum of **3** exhibits the typical emission bands of the Tb^{III} ion due to the chelating hfac⁻ ligand.

When the ligands are introduced to sensitize Dy^{III} ion, both complex **4** ($\lambda_{\text{ex}} = 287$ nm) and Dy(hfac)₃·2H₂O ($\lambda_{\text{ex}} = 285$ nm) (Figure S11, ESI) present no characteristic bands of Dy³⁺ ion, the spectra is dominated by ligand-centered emission, indicating that the ligands cannot transfer energy to Dy^{III} effectively. This is mostly because of close energy gap of the triplet state in the hfac ligand and Dy^{III} (⁴F_{9/2} = 21100 cm⁻¹, $\Delta E = 1100$ cm⁻¹) resulting in poor energy transfer from the hfac⁻ ligands to the Dy^{III} ion.

Magnetic Properties.

The temperature dependence of the magnetic susceptibilities of **2–6** are recorded in the range 2–300 K at 1000 Oe, as depicted in Figure 4. At room temperature, the $\chi_{\text{M}}T$ values of

complexes **2–6** are 15.71, 23.17, 27.80, 27.14 and 22.24 cm³ K mol⁻¹, respectively; the theoretical values for two isolated Ln^{III} cations follow: two Gd^{III} (⁸S_{7/2}, g = 2) are 15.76 cm³ K mol⁻¹ for **2**; two Tb^{III} (⁷F₆, g = 3/2) are 23.64 cm³ K mol⁻¹ for **3**; two Dy^{III} (⁶H_{15/2}, g = 4/3) are 28.34 cm³ K mol⁻¹ for **4**; two Ho^{III} (⁵I₈, g = 5/4) are 28.14 cm³ K mol⁻¹ for **5**; two Er^{III} (⁴I_{15/2}, g = 6/5) are 22.96 cm³ K mol⁻¹ for **6**. All of the values of **2–6** are almost consistent with the expected values.

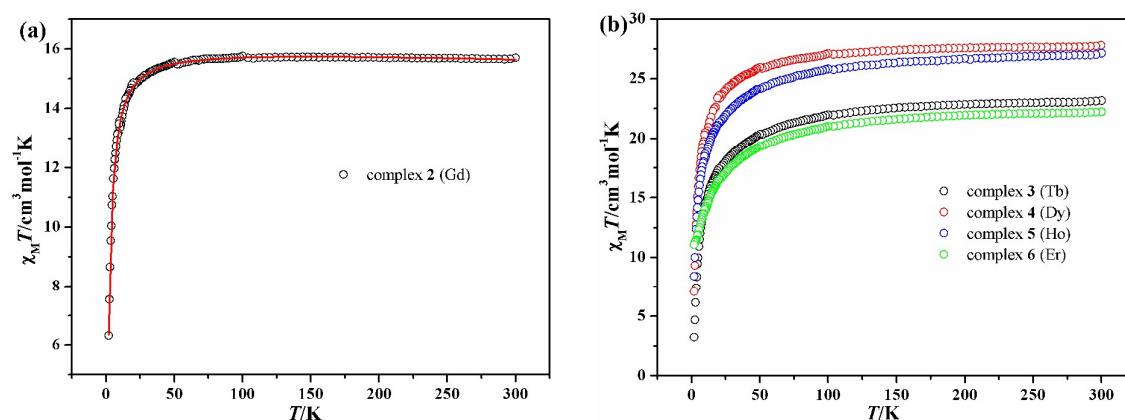


Figure 4. (a) Temperature dependence of the $\chi_M T$ product for **2** [(○) experimental data; (—) best-fit curve]; (b) temperature dependence of $\chi_M T$ for complexes **3–6**.

As the temperature decreases, $\chi_M T$ value of **2** stays essentially constant until ca. 30 K, and then the value decreases rapidly to a minimum of 6.32 cm³ K mol⁻¹ at 2 K. The decrease of $\chi_M T$ at low temperature indicates the presence of weak antiferromagnetic interactions between adjacent Gd^{III} ions. The variable temperature susceptibility data obey the Curie-Weiss law (equation (1)) with $C = 15.79$ cm³ K mol⁻¹, $\theta = -1.24$ K (Figure S12, ESI). The susceptibility data was further analyzed by using equations (2)–(4),

$$\chi = C/(T-\theta) \quad (1)$$

$$\chi_M = (2Ng^2\beta^2 / kT)(A/B) \quad (2)$$

$$A = e^x + 5e^{3x} + 14e^{6x} + 30e^{10x} + 55e^{15x} + 91e^{21x} + 140e^{28x} \quad (3)$$

$$B = 1 + 3e^x + 5e^{3x} + 7e^{6x} + 9e^{10x} + 11e^{15x} + 13e^{21x} + 15e^{28x} \quad (4)$$

which are derived from the isotropic spin Hamiltonian $\hat{H} = -J\hat{S}_A \cdot \hat{S}_B$, where J is the exchange coupling parameter, $x = J/kT$, and \hat{S}_A and \hat{S}_B are the spin operators of the local spins ($\hat{S}_A = \hat{S}_B = 7/2$). The best-fitting results give: $J = -0.078 \text{ cm}^{-1}$ and $g = 2.022$ (Figure 4(a)). The negative θ and J values further confirm the occurrence of weak antiferromagnetic coupling in **2**.

In the cases of **3–6**, $\chi_M T$ values decrease slowly from 300 to ca. 100 K, and then decrease distinctly and reach the minimums of 3.24, 7.09, 8.40 and 11.07 $\text{cm}^3 \text{ K mol}^{-1}$ for **3–6** respectively at 2 K, which may result from the depopulation of the Stark sublevels and/or significant magnetic anisotropy present in Ln^{III} systems.

Magnetization measurements were investigated in the range of 0–8 T at 2–10 K for **2** (Figure 5(a)). The plot of M versus H displays a steady increase with the increasing magnetic field. M reaches a value of $14.07 N\beta$ at 2 K and 8 T, which agrees with the theoretical value of $14 N\beta$ for two Gd^{III} ($g = 2$, $S = 7/2$). Magnetic entropy change ΔS_m , a key parameter in evaluating the MCE, can be derived by applying the Maxwell equation $\Delta S_m(T)_{\Delta H} = \int [\partial M(T, H) / \partial T]_H dH$ to the experimentally obtained magnetization data.²⁵ The entropy changes at various magnetic fields and temperatures are summarized in Figure 5(b), with the maximum value $-\Delta S_m$ of $16.83 \text{ J kg}^{-1} \text{ K}^{-1}$ for $T = 2 \text{ K}$ and $\Delta H = 8 \text{ T}$. The value of $-\Delta S_m$ is smaller than the value of $20.27 \text{ J kg}^{-1} \text{ K}^{-1}$ for two uncoupled Gd^{III} (judged by $2R \ln(2S + 1)$, where R is the gas constant and S is the spin state). The gap between the experimental data and the theoretical value mainly originates from the antiferromagnetic interactions in **2**.²⁶ The observed $-\Delta S_m$ is smaller than that of reported Gd^{III} -based molecular systems,²⁷ close to the

antiferromagnetic $\{\text{Gd}_2\}$ complex ($17.25 \text{ J kg}^{-1} \text{ K}^{-1}$, $\Delta H = 7 \text{ T}$ at 3 K).²⁸

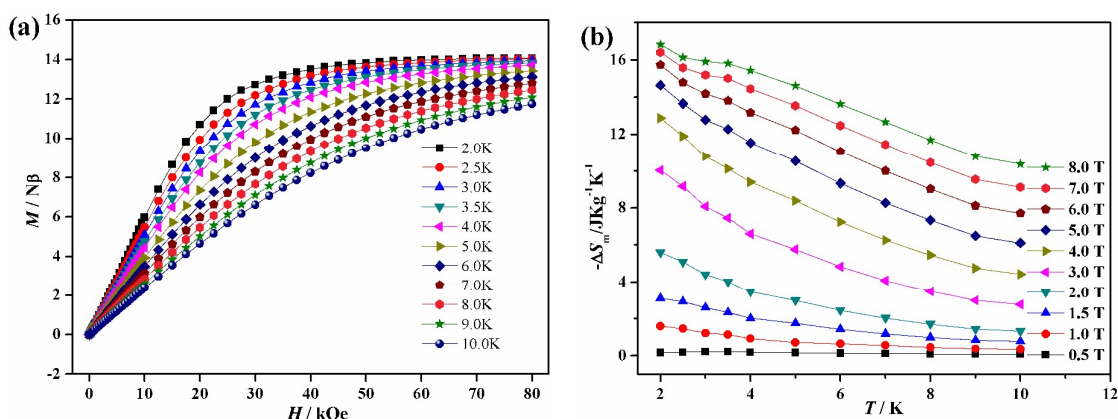


Figure 5. (a) Magnetization versus applied field of **2** at $T = 2.0$ – 10.0 K and $H = 0$ – 8 T ; (b) temperature dependencies of magnetic entropy change ($-\Delta S_m$) as calculated from the magnetization data of **2** at $T = 2$ – 10 K and 0 – 8 T .

To probe the dynamics of the magnetization, alternating current susceptibility measurements were carried out under zero field. From the temperature dependencies of the ac susceptibility (Figure 6), both the in-phase (χ') and out-of-phase (χ'') signals show the frequency dependence maximum, signaling the “freezing” of the spins by the anisotropy barriers, typical features associated with SMM behavior. However, the peaks in out-of-phase (χ'') signals can only be found at frequencies higher than 711 Hz .

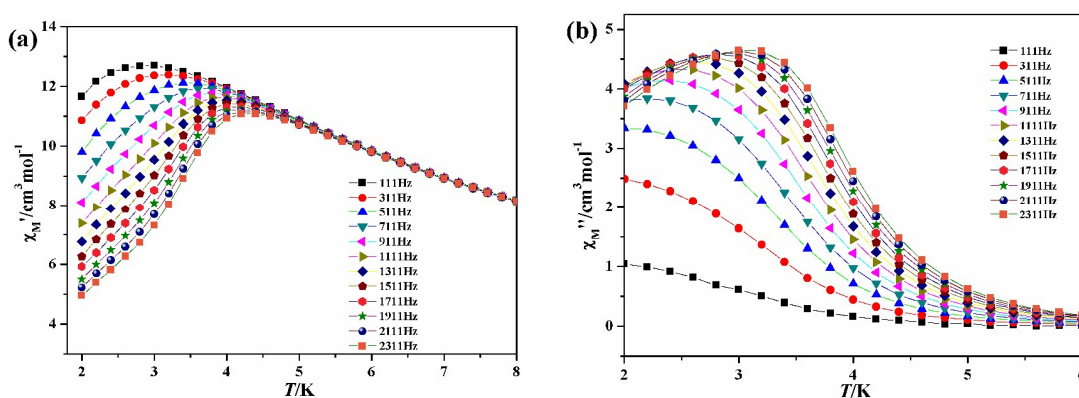


Figure 6. Temperature dependence of the in-phase (a) and out-of-phase (b) components of the ac magnetic susceptibility for **4** in zero dc fields with an oscillation of 3.0 Oe .

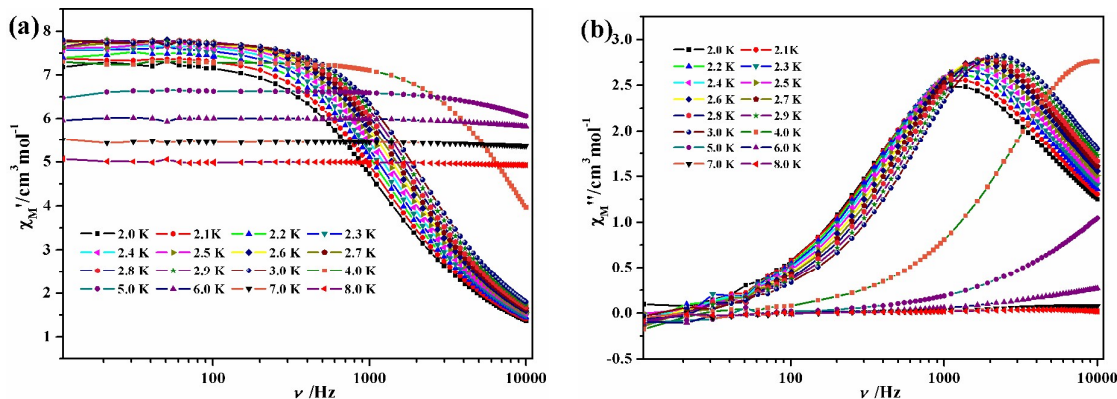


Figure 7. Frequency dependence of the in-phase (a) and out-of phase (b) ac susceptibility for **4** under zero dc field.

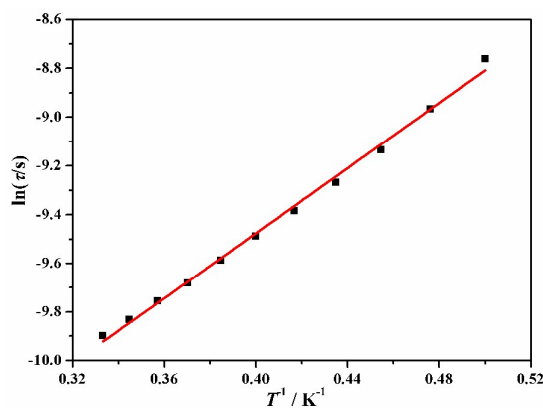


Figure 8. Plot of $\ln(\tau)$ versus T^{-1} fitting to the Arrhenius law for complex **4**.

From frequency dependencies of the ac susceptibility (Figure 7), the magnetization relaxation times (τ) have been estimated between 2 and 3 K (Figure 8). Above 2.1 K, the relaxation follows a thermally activated mechanism affording an energy barrier of 6.7 K with a pre-exponential factor (τ_0) of 5.3×10^{-6} s based on Arrhenius law [$\tau = \tau_0 \exp(U_{\text{eff}}/(kT))$], which is consistent with those reported for similar SMMs (in the range of 10^{-6} – 10^{-11} s).^{29,30} Cole-Cole diagrams (Figure S13, ESI) in the form of χ'' versus χ' with nearly semicircular shapes have also been obtained. These data have been fitted to the generalized Debye model,³¹ giving the small distribution coefficient α value 0.068–0.156 (between 2 and 5 K), indicating the narrow distribution of relaxation times at these temperatures. In a word, the

energy barrier obtained is smaller than that for some complexes, but higher than or comparable to that of other dysprosium complexes reported in the literatures.³² The synthetic approach illustrated in this work may provide opportunities for developing several new polynuclear lanthanide^{III} complexes with interesting magnetic and luminescence properties.

Conclusions

In this work, seven dinuclear rare earth complexes based on 8-hydroxyquinoline Schiff base ligand [RE₂(hfac)₄L₂] (RE = Y (**1**), Gd (**2**), Tb (**3**), Dy (**4**), Ho (**5**), Er (**6**) and Lu (**7**)) have been synthesized. The luminescent emission spectra indicate that complex **3** exhibits characteristic Tb^{III} centered luminescence, while complexes **1** and **7** show luminescence from the L⁻ ligands. The magnetic properties study reveal that **2** features magnetocaloric effect with the magnetic entropy change of $-\Delta S_m = 16.83 \text{ J kg}^{-1} \text{ K}^{-1}$ at 2 K for $\Delta H = 8 \text{ T}$, and **4** shows slow relaxation of the magnetization typical of SMM behavior with anisotropic barrier of 6.7 K, $\tau_0 = 5.3 \times 10^{-6} \text{ s}$. Further magnetic and luminescence properties studies on other polynuclear lanthanide^{III} complexes based on 8-hydroxyquinoline Schiff base ligand are in progress in our laboratory.

Acknowledgments

This work was supported financially by the National Natural Science Foundation of China (Nos. 21271137, 21473121 and 21571138).

Reference

- (a) R. Sessoli and A. K. Powell, *Coord. Chem. Rev.*, 2009, **253**, 2328; (b) Y. N. Guo, G. F. Xu, Y. Guo and J. K. Tang, *Dalton Trans.*, 2011, **40**, 9953; (c) P. Zhang, Y. N. Guo and J. Tang, *Coord. Chem. Rev.*, 2013, **257**, 1728; (d) F. Habib and M. Murugesu, *Chem. Soc.*

- Rev.*, 2013, **42**, 3278; (e) D. N. Woodruff, R. E. P. Winpenny and R. A. Layfield, *Chem. Rev.*, 2013, **113**, 5110; (f) R. J. Blagg, L. Ungur, F. Tuna, J. Speak, P. Comar, D. Collison, W. Wernsdorfer, E. J. L. McInnes, L. F. Chibotaru and R. E. P. Winpenny, *Nat. Chem.*, 2013, **5**, 673; (g) J. W. Sharples and D. Collison, *Coord. Chem. Rev.*, 2014, **260**, 1; (h) L. Ungur, S. Y. Lin, J. K. Tang and L. F. Chibotaru, *Chem. Soc. Rev.*, 2014, **43**, 6894; (i) P. Zhang, L. Zhang and J. K. Tang, *Dalton Trans.*, 2015, **44**, 3923.
- 2 (a) M. Evangelisti and E. K. Brechin, *Dalton Trans.*, 2010, **39**, 4672; (b) E. Cremades, S. Gómez-Coca, D. Aravena, S. Alvarez and E. Ruiz, *J. Am. Chem. Soc.*, 2012, **134**, 10532; (c) P. Shi, G. Xiong, Z. Zhang and B. Zhao, *Sci. China: Chem.*, 2013, **43**, 1262; (d) J. L. Liu, Y. C. Chen, F. S. Guo and M. L. Tong, *Coord. Chem. Rev.*, 2014, **281**, 26.
- 3 (a) P. D. W. Boyd, Q. Li, J. B. Vincent, K. Folting, H. R. Chang, W. E. Streib, J. C. Huffman, G. Christou and D. N. Hendrickson, *J. Am. Chem. Soc.*, 1988, **110**, 8537; (b) A. Caneschi, D. Gatteschi, R. Sessoli, A. L. Barra, L. C. Brunel and M. Guillot, *J. Am. Chem. Soc.*, 1991, **113**, 5873; (c) R. Sessoli, H. L. Tsai, A. R. Schake, S. Wang, J. B. Vincent, K. Folting, D. Gatteschi, G. Christou and D. N. Hendrickson, *J. Am. Chem. Soc.*, 1993, **115**, 1804; (d) R. Sessoli, D. Gatteschi, A. Caneschi and M. A. Novak, *Nature*, 1993, **365**, 141.
- 4 (a) G. Aromi and E. Brechin, *Struct. Bonding*, 2006, **122**, 1; (b) C. J. Milios, A. Vinslava, W. Wernsdorfer, S. Moggach, S. Parsons, S. P. Perlepes, G. Christou and E. K. Brechin, *J. Am. Chem. Soc.*, 2007, **129**, 2754.
- 5 R. L. Carlin, *Magnetochemistry*, Springer, Berlin, 1986.
- 6 (a) Y. Z. Zheng, Y. Lan, W. Wernsdorfer, C. E. Anson and A. K. Powell, *Chem. Eur. J.*, 2009, **15**, 12566; (b) J. Luzon, K. Bernot, I. J. Hewitt, C. E. Anson, A. K. Powell and R.

- Sessoli, *Phys. Rev. Lett.*, 2008, **100**, 247205; (c) J. W. Sharples, Y. Z. Zheng, F. Tuna, E. J. L. McInnes and D. Collison, *Chem. Commun.*, 2011, **47**, 7650; (d) F. Habib, P. H. Lin, J. Long, I. Korobkov, W. Wernsdorfer and M. Murugesu, *J. Am. Chem. Soc.*, 2011, **133**, 8830; (e) Y. Bi, Y. N. Guo, L. Zhao, Y. Guo, S. Y. Lin, S. D. Jiang, J. K. Tang, B. W. Wang and S. Gao, *Chem. Eur. J.*, 2011, **17**, 12476; (f) P. Zhang, L. Zhang, C. Wang, S. F. Xue, S. Y. Lin and J. K. Tang, *J. Am. Chem. Soc.*, 2014, **136**, 4484; (g) Y. N. Guo, L. Ungur, G. E. Granroth, A. K. Powell, C. J. Wu, S. E. Nagler, J. K. Tang, L. F. Chibotaru and D. M. Cui, *Sci. Rep.*, 2014, **4**, 5471; (h) C. Wang, S. Y. Lin, J. F. Wu, S. W. Yuan and J. K. Tang, *Dalton Trans.*, 2015, **44**, 4648.
- 7 (a) J. D. Rinehart, M. Fang, W. J. Evans and J. R. Long, *J. Am. Chem. Soc.*, 2011, **133**, 14236; (b) J. D. Rinehart, M. Fang, W. J. Evans, J. R. Long, *Nat. Chem.*, 2011, **3**, 538.
- 8 F. Tuna, C. A. Smith, M. Bodensteiner, L. Ungur, L. F. Chibotaru, E. J. L. McInnes, R. E. P. Winpenny, D. Collison and R. A. Layfield, *Angew. Chem. Int. Ed.*, 2012, **51**, 6976.
- 9 (a) K. A. Gschneidner Jr. and V. K. Pecharsky, *Int. J. Refrig.*, 2008, **31**, 945; (b) D. Gatteschi and R. Sessoli, *Angew. Chem., Int. Ed.*, 2003, **42**, 268.
- 10 F. S. Guo, J. D. Leng, J. L. Liu, Z. S. Meng and M. L. Tong, *Inorg. Chem.*, 2012, **51**, 405.
- 11 Y. N. Guo, G. F. Xu, W. Wernsdorfer, L. Ungur, Y. Guo, J. K. Tang, H. J. Zhang, L. F. Chibotaru and A. K. Powell, *J. Am. Chem. Soc.*, 2011, **133**, 11948.
- 12 (a) G. Karotsis, S. Kennedy, S. J. Teat, C. M. Beavers, D. A. Fowler, J. J. Morales, M. Evangelisti, S. J. Dalgarno and E. K. Brechin, *J. Am. Chem. Soc.*, 2010, **132**, 12983; (b) A. S. Dinca, A. Ghirri, A. M. Madalan, M. Affronte and M. Andruh, *Inorg. Chem.*, 2012, **51**, 3935.

- 13 (a) M. Evangelisti, O. Roubeau, E. Palacios, A. Camon, T. N. Hooper, E. K. Brechin and J. J. Alonso, *Angew. Chem. Int. Ed.*, 2011, **50**, 6606; (b) L. X. Chang, G. Xiong, L. Wang, P. Cheng and B. Zhao, *Chem. Commun.*, 2013, **49**, 1055; (c) F. S. Guo, Y. C. Chen, L. L. Mao, W. Q. Lin, J. D. Leng, R. Tarasenko, M. Orendac, J. Prokleska, V. Sechovsky and M. L. Tong *Chem. Eur. J.*, 2013, **19**, 14876; (d) J. B. Peng, X. J. Kong, Q. C. Zhang, M. Orendac, J. Prokleska, Y. P. Ren, L. S. Long, Z. P. Zheng and L. S. Zheng, *J. Am. Chem. Soc.*, 2014, **136**, 17938.
- 14 (a) V. Chandrasekhar, S. Hossain, S. Das, S. Biswas and J. P. Sutter, *Inorg. Chem.*, 2013, **52**, 6346; (b) S. F. Xue, Y. N. Guo, L. Zhao, H. X. Zhang and J. K. Tang, *Inorg. Chem.*, 2014, **53**, 8165; (c) L. Zhang, P. Zhang, L. Zhao, J. F. Wu, M. Guo and J. K. Tang, *Inorg. Chem.*, 2015, **54**, 5571; (d) E. M. Pineda, N. F. Chilton, R. Marx, M. Dorfel, D. O. Sells, P. Neugebauer, S. D. Jiang, D. Collison, J. V. Slagereen, E. J. L. McInnes and R. E. P. Winpenny, *Nature Commun.*, 2014, **5**, 5243; (e) W. M. Wang, H. X. Zhang, S. Y. Wang, H. Y. Shen, H. L. Gao, J. Z. Cui and B. Zhao, *Inorg. Chem.*, 2015, **54**, 10610; (f) H. Y. Shen, W. M. Wang, Y. X. Bi, H. L. Gao, S. Liu and J. Z. Cui, *Dalton Trans.*, 2015, **44**, 18893.
- 15 (a) F. Artizzu, P. Deplano, L. Marchio, M. L. Mercuri, L. Pilia, A. Serpe, F. Quochi, R. Orru, F. Cordella, F. Meinardi, R. Tubino, A. Mura and G. Bongiovanni, *Inorg. Chem.*, 2005, **44**, 840; (b) A. O'Riordan, R. Van Deun, E. Mairiaux, S. Moynihan, P. Fias, P. Nockemann, K. Binnemans and G. Redmond, *Thin Solid Films*, 2008, **516**, 5098; (c) M. Iwamuro, T. Adachi, Y. Wada, T. Kitamura, N. Nakashima and S. Yanagida, *Bull. Chem. Soc. Jpn.*, 2000, **73**, 1359; (d) A. Meyers, A. Kimyonok and M. Weck, *Macromolecules*,

- 2005, **38**, 8671.
- 16 (a) M. F. Richardson, W. F. Wagner and D. E. Sands, *J. Inorg. Nucl. Chem.*, 1968, **30**, 1275; (b) K. Bernot, L. Bogani, A. Caneschi, D. Gatteschi and R. Sessoli, *J. Am. Chem. Soc.*, 2006, **128**, 7947.
- 17 (a) T. Hata and T. Uno, *B. C. S. J.*, 1972, **45**, 477; (b) P. Hu, F. S. Wang and G. X. Jin, *Organomet.*, 2011, **30**, 1008.
- 18 CrystalClear, Rigaku Corporation, Woodlands, TX, USA, 1999.
- 19 G. M. Sheldrick, *Acta Crystallogr., Sect. A: Found. Crystallogr.*, 2008, **64**, 112.
- 20 (a) S. W. Zhang, J. W. Zhao, P. T. Ma, H. N. Chen, J. Y. Niu and J. P. Wang, *Cryst. Growth Des.*, 2012, **12**, 1263; (b) A. J. Gaunt, I. May, M. J. Sarsfield, D. Collison, M. Helliwell and I. S. Dennis, *Dalton Trans.*, 2003, 2767; (c) W. T. Xu, Y. F. Zhou, D. C. Huang, W. Xiong, M. Y. Su, K. Wang, S. Han and M. C. Hong, *Cryst. Growth Des.*, 2013, **13**, 5420.
- 21 (a) S. Liu, L. Gelmini, S. J. Rettig, R. C. Thompson and C. Orvig, *J. Am. Chem. Soc.*, 1992, **114**, 6081; (b) L. E. Roy and T. Hughbanks, *J. Am. Chem. Soc.* 2006, **128**, 568; (c) J. Long, F. Habib, P. H. Lin, I. Korobkov, G. Enright, L. Ungur, W. Wernsdorfer, L. F. Chibotaru and M. Murugesu, *J. Am. Chem. Soc.*, 2011, **133**, 5319.
- 22 G. A. Crosby, R. M. Alire and R. E. Whan, *J. Chem. Phys.*, 1961, **34**, 743.
- 23 M. Latva, H. Takalo, V. M. Mikkala, C. Matachescu, J. C. Rodriguez-Ubis and J. Kankare, *J. Lumin.*, 1997, **75**, 149.
- 24 H. B. Xu, J. Li, L. X. Shi and Z. N. Chen, *Dalton Trans.*, 2011, **40**, 5549.
- 25 (a) M. Evangelisti, A. Candini, A. Ghirri, M. Affronte, E. K. Brechin and E. J. McInnes, *L.*

- Appl. Phys. Lett.*, 2005, **87**, 072504; (b) M. Manoli, R. D. L. Johnstone, Parsons, S. M. Murrie, M. Affronte, M. Evangelisti and E. K. Brechin, *Angew. Chem., Int. Ed.*, 2007, **119**, 4440; (c) R. Shaw, R. H. Laye, L. F. Jones, D. M. Low, C. Talbot-Eeckelaers, Q. Wei, C. J. Milios, S. Teat, M. Helliwell, J. Raftery, M. Evangelisti, M. Affronte, D. Collison, E. K. Brechin and E. J. L. McInnes, *Inorg. Chem.*, 2007, **46**, 4968.
- 26 (a) Y. C. Chen, F. S. Guo, Y. Z. Zheng, J. L. Liu, J. D. Leng, R. Tarasenko, M. Orendáč, J. Prokleška, V. Sechovský and M. L. Tong, *Chem. Eur. J.*, 2013, **19**, 13504; (b) J. B. Peng, Q. C. Zhang, X. J. Kong, Y. P. Ren, L. S. Long, R. B. Huang, L. S. Zheng and Z. Zheng, *Angew. Chem., Int. Ed.*, 2011, **50**, 10649.
- 27 (a) Y. Z. Zheng, G. J. Zhou, Z. P. Zheng and R. E. P. Winpenny, *Chem. Soc. Rev.*, 2014, **43**, 1462; (b) S. W. Zhang, W. Shi, L. L. Li, E. Y. Duan and P. Cheng, *Inorg. Chem.*, 2014, **53**, 10340.
- 28 S. Biawas, H. S. Jena, S. Goswami, S. Sanda and S. Konar, *Cryst. Growth Des.*, 2014, **14**, 1287.
- 29 (a) L. F. Zou, L. Zhao, Y. N. Guo, G. M. Yu, Y. Guo, J. K. Tang and Y. H. Li, *Chem. Commun.*, 2011, **47**, 8659; (b) M. Fang, J. J. Li, P. F. Shi, B. Zhao and P. Cheng, *DaltonTrans.*, 2013, **42**, 6553; (c) G. Xiong, X. Y. Qin, P. F. Shi, Y. L. Hou, J. Z. Cui and B. Zhao, *Chem. Commun.*, 2014, **50**, 4255; (d) M. Fang, H. H. Zhao, A. V. Prosvirin, D. Pinkowicz, B. Zhao, P. Cheng, W. Wernsdorfer, E. K. Brechin and K. R. Dunbar, *DaltonTrans.*, 2013, **42**, 14693; (e) Y. L. Hou, G. Xiong, P. F. Shi, R. R. Cheng, J. Z. Cui and B. Zhao, *Chem. Commun.*, 2013, **49**, 6066.
- 30 (a) N. Ishii, Y. Okamura, S. Chiba, T. Nogami and T. Ishida, *J. Am. Chem. Soc.*, 2008,

- 130**, 24; (b) K. S. Gavrilenko, O. Cador, K. Bernot, P. Rosa, R. Sessoli, S. Golhen, V. V. Pavlishchuk and L. Ouahab, *Chem. Eur. J.*, 2008, **14**, 2034.
- 31 (a) J. A. Mydosh, *Spin Glasses: An Experimental Introduction*; Taylor & Francis: London, 1993; (b) W. E. Buschmann, J. Ensling, P. Gülich and J. S. Miller, *Chem. Eur. J.*, 1999, **5**, 3019; (c) D. Gatteschi, R. Sessoli and J. Villain, *Molecular Nanomagnets*; Oxford University Press: New York, 2006; pp 69–75; (d) T. Yamaguchi, Y. Sunatsuki, H. Ishida, M. Kojima, H. Akashi, N. Re, N. Matsumoto, A. Pochaba and J. Mroziński, *Inorg. Chem.*, 2008, **47**, 5736.
- 32 (a) J. B. Peng, X. J. Kong, Y. P. Ren, L. S. Long, R. B. Huang and L. S. Zheng, *Inorg. Chem.*, 2012, **51**, 2186; (b) S. K. Langley, N. F. Chilton, I. A. Gass, B. Moubaraki and K. S. Murray, *Dalton Trans.*, 2011, **40**, 12656; (c) P. F. Shi, Y. Z. Zheng, X. Q. Zhao, G. Xiong, B. Zhao, F. F. Wan and P. Cheng, *Chem. Eur. J.*, 2012, **18**, 15086; (d) E. C. Mazarakioti, K. M. Poole, L. Cunha-Silva, G. Christou and T. C. Stamatatos, *Dalton Trans.*, 2014, **43**, 11456.

Table of contents

Seven dinuclear complexes based on 8-hydroxyquinoline Schiff base derivatives and β -diketone ligands have been synthesized, structurally and magnetically characterized.

